Matter

CellPress

Article

Photo-stable, 1D-nanofilaments TiO_2-based lepidocrocite for photocatalytic hydrogen production in water-methanol mixtures

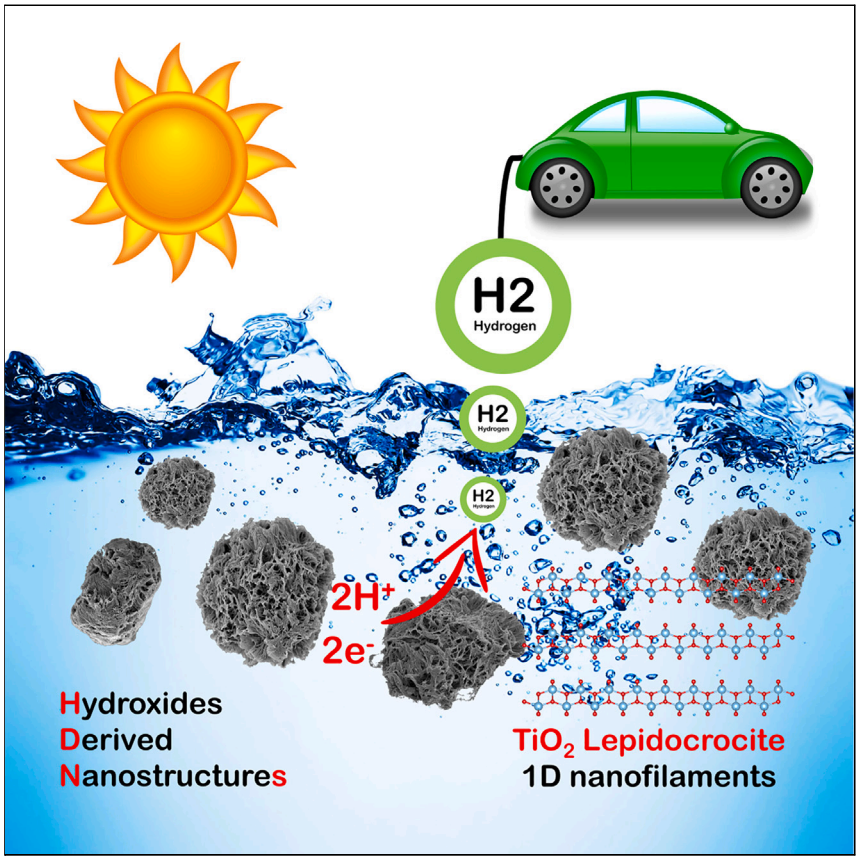

To convert sunlight to hydrogen, cheap, active, and stable photocatalysts are required. Recently, we discovered a one pot method to convert inexpensive Ti-based compounds into one-dimensional titania-based nanostructures in the 50°C–80°C temperature range and ambient pressure. The new materials are quite efficient in converting sunlight to hydrogen and are exceptionally stable in water/methanol mixtures. These facts bode well for the use of these materials to produce green hydrogen from the sun commercially in the near future.

Benchmark
First qualification/assessment of material properties and/or performance

Hussein O. Badr, Varun Natu, Ștefan Neațu, ..., Matthew Racey, Michel W. Barsoum, Mihaela Florea

stefan.neatu@infim.ro (Ș.N.)
barsoumw@drexel.edu (M.W.B.)
mihaela.florea@infim.ro (M.F.)

Highlights

Scalable, cheap, one-pot, facile synthesis of titanium oxide-based nanofilaments

Our nanofilaments outperform commercial P25 in both activity and stability

Our discovery represents an important step for the large-scale production of green hydrogen from sunlight

Badr et al., Matter 6, 1–17
September 6, 2023
https://doi.org/10.1016/j.matt.2023.05.026

Please cite this article in press as: Badr et al., Photo-stable, 1D-nanofilaments TiO_2-based lepidocrocite for photocatalytic hydrogen production in water-methanol mixtures, Matter (2023), https://doi.org/10.1016/j.matt.2023.05.026

Matter

CellPress

Article

Photo-stable, 1D-nanofilaments TiO_2-based lepidocrocite for photocatalytic hydrogen production in water-methanol mixtures

Hussein O. Badr,[1] Varun Natu,[1,2] Ștefan Neațu,[3,*] Florentina Neațu,[3] Andrei Kuncser,[3] Arpad M. Rostas,[3] Matthew Racey,[1] Michel W. Barsoum,[1,4,*] and Mihaela Florea[3,*]

SUMMARY

Water and sunlight are the cleanest, most renewable, and abundant resources on Earth. Developing inexpensive, scalable photocatalysts that are highly stable for hydrogen (H_2) production has long been a cherished dream of humanity. Herein, we report on one-dimensional lepidocrocite-based sub-nanofilaments (NFs), ≈ 5 × 7 Å^2 in cross-section, that generate H_2 from 80:20 v/v water/methanol mixtures when illuminated by simulated sunlight. The NFs were stable in the mixtures for times >4,300 h, 300 h of which were under irradiation. Apparent quantum yields as high as 11.7% were obtained. Based on deuterated water results, we conclude that water is the H_2 source. Further, no carbon dioxide (CO_2) due to photocatalytic degradation of methanol was detected. Therefore, the NFs have strong green credentials and lucrative economic prospects for large scale up. We expect these NFs will lead to new lines for developing cheap and ultra-stable materials to produce H_2 photochemically for a long time.

INTRODUCTION

Although hydrogen (H_2) is the most abundant element in the universe, its current use in energy production is small.[1] However, it has long been appreciated that some photocatalysts exposed to sunlight can split water to produce H_2. The light creates electron-hole pairs—needed to produce H_2 and oxygen (O_2)—before recombining. As the photogenerated electron-hole pairs initiate simultaneous oxidation and reduction reactions at the photocatalyst's outer surfaces, the consumption rate of electrons and holes must be equal to maintain charge neutrality during the process. For this reason, most of the studies on H_2 evolution reactions (HERs) are carried out with an excess of reagents such as methanol that act as hole quenchers.[2] Thus, while holes are quenched and used by different hole scavengers, the electrons undergo efficient HER through the reduction of H^+ species followed by the formation of intermediate adsorbed H* states and, finally, the production of H_2 molecules.[3] Based on these principles, considerable efforts have been devoted to splitting water at the lowest cost possible using a variety of photocatalytic systems.[4]

For the past five decades, various semiconductor materials, such as TiO_2, $SrTiO_3$, CdS, $BiVO_4$, Ta_3N_5, TaON, g-C_3N_4, and Ag_3PO_4, have been studied. Further, their nanostructured assemblies, composites with other one-dimensional (1D) and two-dimensional (2D) functional materials, and decorating with platinum (Pt) group metal nanoparticles, have been extensively studied to improve their photocatalytic properties.[5,6] Despite considerable effort, currently, no commercially available materials

PROGRESS AND POTENTIAL

Water and sunlight are the cleanest, most renewable, and abundant resources on Earth. Using photocatalysts, one can absorb sunlight and split water to its constituting elements, oxygen and hydrogen. The latter is a green fuel that is currently being developed to replace fossil fuel so that we can reduce carbon dioxide (CO_2) emissions. In this work, we used one-dimensional titanium oxide-based photocatalyst (a novel nanostructured material we recently discovered) to produce hydrogen from a water/alcohol mixture. Our titanium oxide nanostructures generate about an order of magnitude higher H2 gas than their commercial titanium oxide (P25) counterpart. Moreover, our photocatalyst was found to be stable in water for 6 months, 12 days of which the photocatalyst was under illumination of two artificial suns.

Please cite this article in press as: Badr et al., Photo-stable, 1D-nanofilaments TiO_2-based lepidocrocite for photocatalytic hydrogen production in water-methanol mixtures, Matter (2023), https://doi.org/10.1016/j.matt.2023.05.026

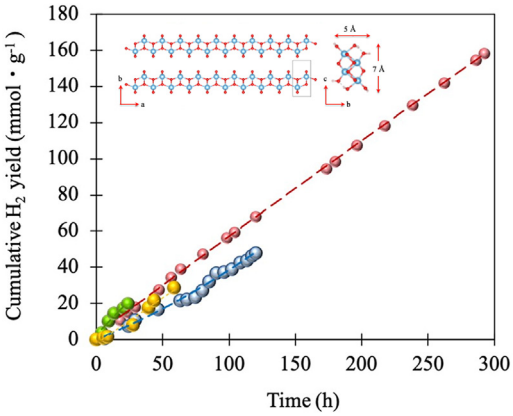

Figure 1. Time dependence of cumulative H_2 yield in H_2O/MeOH mixtures for TCO samples

TCO1 (yellow dots), TCO2 (red dots), TCO3 (blue dots), and TCO4 (green dots). Reaction conditions: 25 mg of photocatalyst dispersed in a 25-mL mixture of DI H_2O and MeOH at 4:1 v/v, 6 h of reaction. Inset shows titanium oxide lepidocrocite-based NFs atomic structures along the growth *a* direction (left) and in cross-section (right).

meet all the requisite requirements for large-scale adoption, viz. high light quantum efficiency, stability, safety, and low cost. From a cost perspective, H_2 generated from photocatalysis is currently estimated to cost ≈\$10 kg^{-1}, with the highest contribution coming from the cost of the photocatalyst itself. At the same time, H_2 produced by fossil fuel reforming—which is not green—costs around \$1 kg^{-1}. For photocatalysis to be competitive, its price must drop roughly an order of magnitude or more for the solar-H_2 world economy to be realized.

We recently discovered that, when powders of more than a dozen Ti-containing precursors, such as TiC, Ti_3SiC_2, TiB_2, and TiN, are immersed in tetramethylammonium hydroxide (TMAH) aqueous solution at 50°C–80°C for a few days, they are transformed into 1D lepidocrocite-based nanofilaments (NFs).[7] In our first report, we concluded the structure of the NFs was anatase.[7] In a more in-depth study, we concluded the structure is lepidocrocite based, which turns into anatase under high Raman laser power.[8] These 1D lepidocrocite nanofilaments hereafter are referred to as just NFs. When anatase TiO_2 powder was used as a precursor and subjected to a similar TMAH treatment, it formed anatase nanoparticles (NPs) instead of NFs. Note the difference in NFs and NPs hereon.

The NFs that form are unique in many respects. First, their X-ray diffraction (XRD) diffractograms are unlike any other TiO_2-based ones in that many fundamental and distinctive TiO_2 peaks are missing.[7,8] Their Raman signature, however, is that of lepidocrocite.[8] Second, with cross-sections in the ≈ 5 × 7 $Å^2$ range that grow in the [200] direction, they are truly 1D (inset in Figure 1).

Any effects on the choice of precursor powder (TiC, TiB_2, TiN, Ti_3SiC_2, etc.) on the NFs cannot be discerned at the XRD, X-ray absorption near-edge structure (XANES), scanning electron microscopy (SEM), or even X-ray photoelectron spectroscopy (XPS) levels.[7] As shown herein, however, the precursor's nature plays a role, as does the temperature of NFs' synthesis.

In this work, we measured the capacity of NFs prepared from TiC, Ti_3SiC_2, TiB_2, and anatase to produce H_2 from H_2O/MeOH mixtures.

RESULTS AND DISCUSSION

Photocatalytic behavior

Table 1 summarizes H_2-production rates (HPRs) for 10 catalysts that were tested under 2 suns irradiation. The first five entries refer to TCOs and TB1, which are NFs

[1]Department of Material Science and Engineering, Drexel University, Philadelphia, PA, USA

[2]Physical and Materials Chemistry Division, CSIR-National Chemical Laboratory, Pune, Maharashtra 411008, India

[3]National Institute of Materials Physics, 405A Atomistilor Street, 077125 Magurele, Romania

[4]Lead contact

*Correspondence: stefan.neatu@infim.ro (Ş.N.), barsoumw@drexel.edu (M.W.B.), mihaela.florea@infim.ro (M.F.)

https://doi.org/10.1016/j.matt.2023.05.026

Please cite this article in press as: Badr et al., Photo-stable, 1D-nanofilaments TiO_2-based lepidocrocite for photocatalytic hydrogen production in water-methanol mixtures, Matter (2023), https://doi.org/10.1016/j.matt.2023.05.026

Table 1. HPRs as a function of catalyst under 2 suns irradiation

Entry	Precursor composition	Processing of TCO temperature (°C)[a]	Photocatalyst code	H_2 production rate ($\mu mol \cdot g^{-1} \cdot h^{-1}$)[b]	AQY (%)[c]
1	Ti_3SiC_2	50	TCO1	808	4.6
2	TiC	50	TCO2	598	3.4
3	TiC	80	TCO3	631	11.7
4	TiC	95	TCO4	1,014	5.3
5	TiB_2	80	TB1	296	2.9
6	TiO_2	80	TO1	63	0.4
7	TiO_2	–	P25	180	1.02
8	Ti_3SiC_2	–	Ti_3SiC_2	15	0.1
9	TiC	–	TiC	0	0
10	$Ti_3C_2T_x$	–	$Ti_3C_2T_x$	0	0

The first 6 entries refer to NFs and NPs; the last 4 refer to catalysts used with the composition shown.
[a]Temperatures at which precursors were transformed into NFs.
[b]Reaction conditions: 25 mg of solid material dispersed in 25 mL of a mixture of DI H_2O and MeOH in a 4:1 vol ratio, 6 h of reaction. Irradiation with a Xe lamp (MAX-303 illuminator, Asahi Spectra, Japan) equipped with a UV-vis mirror module (250–650 nm).
[c]Method to calculate the AQYs is described in experimental procedures section.

derived from different precursors. For example, TCO1 was prepared from Ti_3SiC_2, while TCO2, TCO3, and TCO4 were prepared from TiC treated in TMAH at different temperatures: 50°C, 80°C, and 95°C, respectively. For entry 6, we started with anatase powder; the final product was anatase NPs.[7] Entry 7 was TiO_2 P25 powder, which was tested as received. Entries 8 and 9 were TiC, and Ti_3SiC_2 precursors tested directly. While entry 10 is for $Ti_3C_2T_z$ MXene, which was tested as it is also derived from a MAX phase, albeit using a different chemical process.

In addition to HPRs, Table 1 lists the apparent quantum yields (AQYs) of the catalysts tested. All NFs (entries 1–5 in Table 1), except TO1 NPs (entry 6 in Table 1), produced H_2 with AQYs >2.9%. TiO_2 P25 has a higher photocatalytic activity than TO1 (entries 6 and 7 in Table 1). The precursors (entries 8 and 9 in Table 1) were inactive. The same was true of $Ti_3C_2T_x$ MXene (entry 10 in Table 1). Interestingly, the photocatalytic activity of TCOs prepared from TiC depended on the reaction temperatures used during the synthesis of the NFs, with the highest HPR obtained on TCO4. However, for this sample, the AQY was only 5.3% because we have to consider the number of incident photons per second (see Equations 1 and 2 in Experimental procedures). The highest AQY was obtained for TCO3. This value is about one order of magnitude higher than the one obtained when P25 was used (compare entries 3 and 7 in Table 1). Also, the AQYs for the NFs excluding TCO3 all lie between ≈3 and 5.5 (entries 1–5 in Table 1), which are all higher than P25.

Water splitting, in the absence of MeOH, was also explored, and the results are presented in Table S1. Here unreacted TiC and P25 were totally inactive (entries 3 and 4 in Table S1), while the NFs were able to produce H_2 but at nominal rates compared with MeOH-containing mixtures (entries 1 and 2 in Table S1 and Table 1, respectively).

The cumulative H_2 production as a function of time for samples TCO1–TCO4 are plotted in Figure 1 (column 4 in Table 1 lists the codes for the various samples). As impressive as the AQYs of our materials are, their stabilities are truly outstanding as well (see Figure 1). For all samples, no reduction in the HPR was observed with time. For instance, the TCO2 sample is still very active even after >4,300 h (180 days) in H_2O/MeOH mixture, 300 h of which were under 2 suns irradiation while

Please cite this article in press as: Badr et al., Photo-stable, 1D-nanofilaments TiO_2-based lepidocrocite for photocatalytic hydrogen production in water-methanol mixtures, Matter (2023), https://doi.org/10.1016/j.matt.2023.05.026

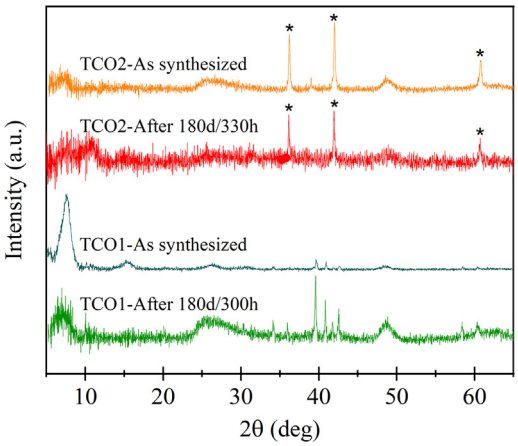

Figure 2. Powder XRD patterns of TCO samples before and after photocatalysis in H_2O/MeOH mixtures for times indicated on graphs; first number is the total time in days, second is under illumination in hours. Low angle peaks are 0k0 peaks

Peaks denoted by asterisks belong to unreacted precursors, Ti_3SiC_2 (for TCO1) or TiC (for TCO2).

being stirred (Figure 1, red dots). Figures S1A and S1B evidence the stability of the HPRs with time after successive evacuations for sample TCO1. We also determined the optimum photocatalyst concentration to be ≈1 g L^{-1} (see Figure S1C).

Other evidence for the stability of TiC-derived NFs are the results shown in Table S2, where the time dependencies of the AQYs are listed. We can observe that, for TCO3 and TCO4, the AQY measured, for the same reaction conditions as in Table 1, remained constant after being in the water for 79 days and 36 days, respectively. Interestingly, the AQY increases with time for the TCO2 sample.

Materials characterization

To confirm the stability of our NFs, we carried out a battery of tests on samples before and after exposure to the Xe light and storage in the H_2O/MeOH mixtures. Powder XRD patterns of samples TCO1 and TCO2, before and after being irradiated for 300 and 330 h, respectively, are shown in Figure 2. As discussed in our most recent work,[8] the XRD signature of our NFs' structure is the presence of three diffraction peaks, at 2θ vlaues ≈26°, ≈48°, and ≈62°, together with the total absence of peaks characteristic of 2D lepidocrocite, most notably the prominent (103) peak at 29° 2θ.[9] In other words, whenever *only* three peaks, corresponding to the 110, 200, and 002 planes of lepidocrocite, are observed, we are dealing with its 1D version. Note that, typically, XRD patterns of lepidocrocite do not show much of a peak at ≈26° 2θ. However, the presence of the lepidocrocite phase seems to be of critical importance for this work, since the TO1 sample—composed of anatase NPs—has an AQY of 0.4% (entry 6 in Table 1).

The XRD patterns of TCO1 and TCO2 contained small amounts of unreacted precursor (TiC or Ti_3SiC_2, denoted in Figure 2 by asterisks). However, since these were found to be photo-catalytically inactive (entries 8 and 9 in Table 1), the reported AQYs must correspond to the NFs. It should be noted that, given the poor crystallinity of the NFs, as seen by the large full width at half maximum (FWHM) of the peaks associated with the lepidocrocite phase, it is currently not possible to quantify the impurity percentage using XRD.

From the diffractograms presented in Figure 2, there were no other apparent changes after exposure to the light besides a possible broadening of the peak at 25° 2θ and the loss in intensity of the 0k0 peaks around 7.5° 2θ. The broadening is an indication that the domain size decreased with time and exposure and is

Please cite this article in press as: Badr et al., Photo-stable, 1D-nanofilaments TiO_2-based lepidocrocite for photocatalytic hydrogen production in water-methanol mixtures, Matter (2023), https://doi.org/10.1016/j.matt.2023.05.026

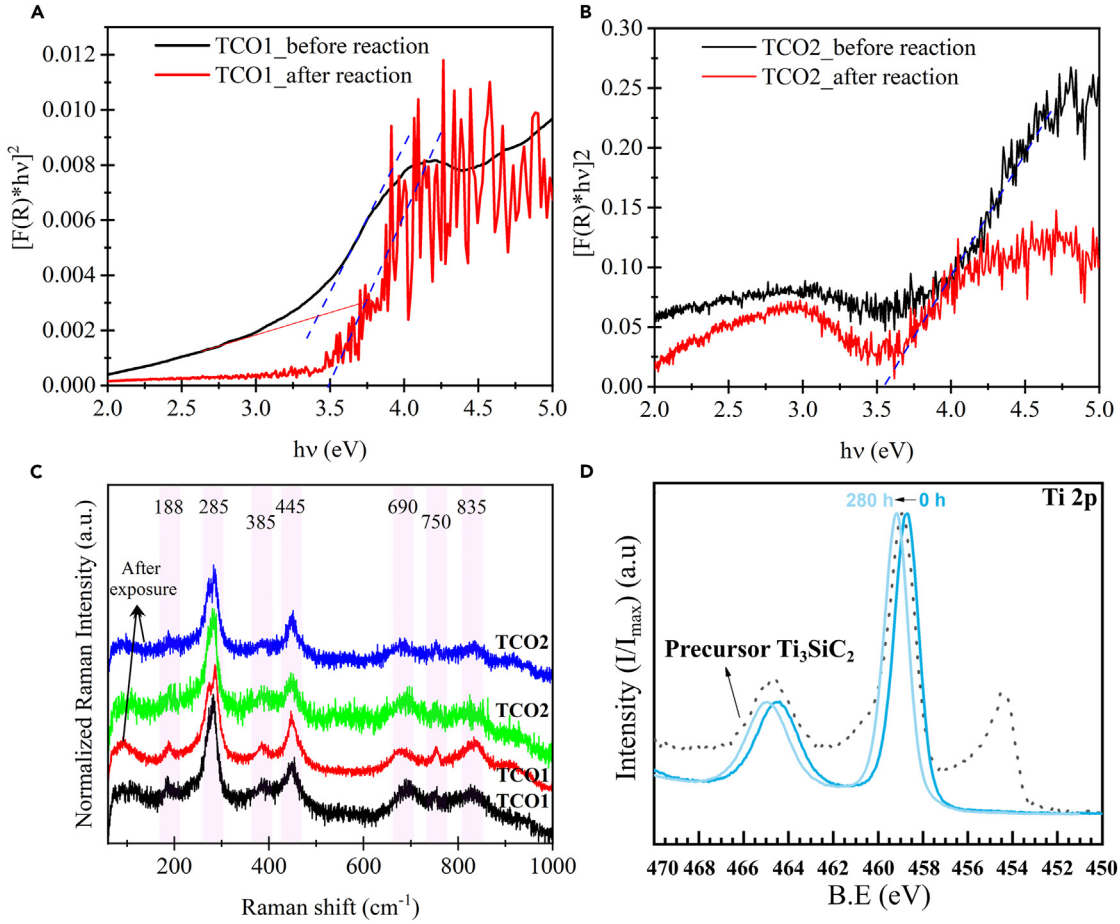

Figure 3. UV-Vis, Raman, and XPS characterization

(A–C) Effect of exposure to Xe light and H_2O/MeOH mixtures on samples TCO1 and TCO2 on (A and B) Tauc plots, (C) Raman spectra before exposure (black and green), and after exposure to light (red and blue). All peaks belong to lepidocrocite.

(D) High-resolution XPS spectra of Ti 2p region before (dark blue) and after (light blue) light exposure for 62 h. Total time in H_2O/MeOH mixtures 33 days. Dotted line shows Ti 2p XPS spectrum of the Ti_3SiC_2 precursor for comparison.

consistent with the low-angle peaks' intensity reduction, which implies that the NF's order along the *b* direction (inset in Figure 1) is reduced after photocatalysis. This is not surprising given that the catalyst powders are dispersed in the H_2O/MeOH mixture and stirred. Notably, the XRD pattern of TCO2 after 6 months in the H_2O/MeOH mixture is devoid of most peaks except three small peaks belonging to the TiC precursor. Note that the increase in intensity of the precursor peaks after photocatalysis does *not* imply their formation; it is simply a reflection of the loss of the order of the NFs. A similar conclusion can be reached for samples TCO3 and TCO4 (see Figures S2A and S2B). Based on the XRD results, it is reasonable to conclude that the NF structure was maintained during the photocatalysis. Still, their initial self-assembly, in which 2D sheets were formed from 1D NFs, appears to be disrupted, leading to partially disentangled NFs. This conclusion is bolstered by transmission electron microscopy (TEM) and XPS results shown below.

To measure the band gap energy (E_g) changes during the prolonged photocatalysis reaction, we plotted Tauc plots.[10,11] These plots, before and after 300 h of irradiation for samples TCO1 and TCO2, are shown in Figures 3A and 3B, respectively. The corresponding plots of TCO3 and TCO4 are presented in Figure S3. As

Please cite this article in press as: Badr et al., Photo-stable, 1D-nanofilaments TiO_2-based lepidocrocite for photocatalytic hydrogen production in water-methanol mixtures, Matter (2023), https://doi.org/10.1016/j.matt.2023.05.026

seen, the E_g remains fairly unchanged in the case of TCOs derived from TiC (TCO2–TCO4). However, for the TCO1 sample (derived from Ti_3SiC_2), a slight increase, ≈0.1 eV, in E_g is observed after photocatalysis. These results, when combined with the XPS, suggest that, after prolonged photocatalysis reaction, all TCO samples are oxidized, and the extent to which they oxidized correlated with the magnitude of the E_g change observed (see Figure 3D). On the other hand, it should be noted that the TCO2 sample shows the presence of some defects or structural disorder of phonon states given by the presence of an Urbach tail.[12]

Figure 3C plots typical Raman spectra before (black and green) and after (red and blue) 300 h of irradiation and 180 total days in our water/MeOH mixture for samples TCO1 and TCO2, respectively. Not only do all peaks in the spectra belong to lepidocrocite[13] but there is little difference between the as-prepared powders and those subjected to light and stirring. The same is true of samples TCO3 and TCO4 (Figure S4). These findings are of crucial importance, and cannot be emphasized enough, because they indicate that, while loss of order along the stacking direction may be occurring (Figure 2), the fundamental building block, presumably 1D lepidocrocite, 1DL, snippets made of TiO_6 octahedra, is preserved. These results, probably more than anything else, confirm the high stability of our NFs. We note in passing that the spectra are noisy because powders were used, and we did not want to focus the laser on any one spot for a long time so as to not induce a transformation to anatase (Figure S5).

Figure 3D plots the Ti 2p XPS peaks before (dark blue curve) and after (light blue curve) 62 h of irradiation for sample TCO1. The binding energies (BEs) of the Ti $2p_{3/2}$ peaks increase from ≈458 to 458.8 eV, which is evidence for Ti^{4+}. For sample TCO2, the BEs (≈458.7 eV) of the Ti $2p_{3/2}$ peak were the same before and after photocatalysis (Figures S8Ai and S8Bi), suggesting this sample was pre-oxidized before testing. What is of critical importance is that, in all cases, the BEs of the Ti $2p_{3/2}$ peaks *after* irradiation are where the Ti surface oxides of the precursor powders line up, viz. fully oxidized. In short, not surprisingly, photocatalysis results in the oxidation of the TCO powders. Crucially, this oxidation does *not* result in a decrease in HPRs.

A comprehensive set of XPS spectra for many samples tested, as well as the precursors, TiC and Ti_3SiC_2, are shown in Figures S6–S8. Apart from the oxidation of Ti in the TiCO1 sample (Figure 3D), changes in the valence band spectra of these samples before and after (Figures S7Aiii and S7Biii) photocatalysis reaction show changes in the electronic states of the sample. This is in line with the Tauc plots (Figure 3A), which also show differences in the bandgap of samples after photocatalysis. Similar changes in the Fermi edge of TCO2 samples are also observed (Figures S8Aiii and S8Biii), but the changes are much more subtle compared with TCO1.

Silicon (Si) which originates in the Ti_3SiC_2 precursor, was also detected in TCO1 samples (Figures S7Aiv and S7Biv). Before catalysis, the Si 2p peak is centered around 102 eV (Figure S7A iv), which is 2.5 eV higher than the 99.5-eV peak ascribed to the Ti–Si–C bond in the Ti_3SiC_2 precursor (Figure S6G), but 1 eV lower than the 103-eV peak typically observed in SiO_2. This implies that there is also some Si doping in the TCO1 samples. The Si also appears stable against oxidation as its BE does not shift after photocatalysis (compare Figures S7Aiv and S7Biv).

Electron paramagnetic resonance (EPR) experiments on samples before and after photocatalysis were also carried out to probe the Ti cations' oxidation states. The EPR spectra recorded in X band (9.87 GHz) are presented in Figure 4. Commercial TiC has no

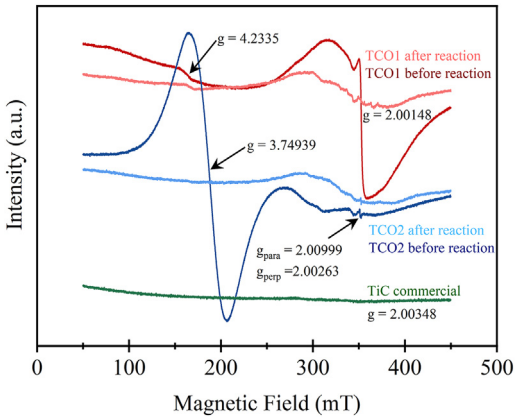

Figure 4. EPR spectra of TCO1 and TCO2 samples before and after irradiation

Also shown for comparison is the EPR spectrum of the TiC precursor.

paramagnetic centers, as seen in the bottom graph in Figure 4. Conversely, the TCO samples show complex EPR signals. First, in the high field region, the TCO1 sample has an intense sharp signal with g = 2.00148, superimposed on a very broad signal, which could originate from Ti^{2+} ions with an electron spin S = 1. We assign the broad line to the (Ms = –l) to (Ms = 0) and (Ms = 0) to (Ms = +1) transitions and the sharp line to the (Ms = −1) to (Ms = +1) double-quantum transition, which is not broadened by crystalline strains and imperfections, in the first order. The same situation is encountered for a ($3d^8$) ion in octahedral symmetry.[14] On the other hand, the TCO2 sample does not present this type of signal; it only presents a weak signal similar to the one observed for MXenes, which is usually associated with some defects.[15] This observation agrees with the UV-visible (UV-vis) measurements (see Figure 3B).

In the lower field region, the TCO1 sample has an isotropic EPR with a g value of 4.23, which is probably that for Ti^{3+}.[16] Sample TCO2 has a very characteristic low field EPR signal with a g value of 3.749, which, as far as we are aware, has not been reported in the literature to date. Since previous measurements indicate the presence of Ti^{3+} ions in the structure, we tentatively associate this EPR signal to Ti^{3+} trapped in a highly symmetrical environment. After irradiation, for all TCO samples tested, the EPR signal intensities either drop significantly or disappear entirely, as the X-band spectra show, indicating that the main oxidation state of Ti ions is 4+, which is EPR silent.

To summarize this section, it is clear that, whatever the Ti average oxidation state of the starting powders, at the end of the photocatalysis, the oxidation state is 4+.

Going further with the morphological characterization of our materials, Figure 5A shows a TEM micrograph of typical long NFs composed of shorter 1DL segment. These, in turn, are composed of NFs, 5 × 7 $Å^2$ in cross-section.[8] Corresponding selected area diffraction (SAD) patterns (Figure 5B) reveal TCO diffraction rings identical to our previous work,[7,8] with the critical difference that now the first ring/arcs are due to the (110) planes, and the second set are due to (200) planes of lepidocrocite.[8]

Typical TEM micrographs of select samples—noted on panels—before and after photocatalysis are shown in Figure 5C–H. Based on these, the following is noteworthy:

(1) As noted above, the as-received material comprises NFs that self-assemble into 2D flakes. In some SAD patterns, the self-alignment is manifested in the form of arcs (insets in Figures 5F and 5G). Rings, however, are also

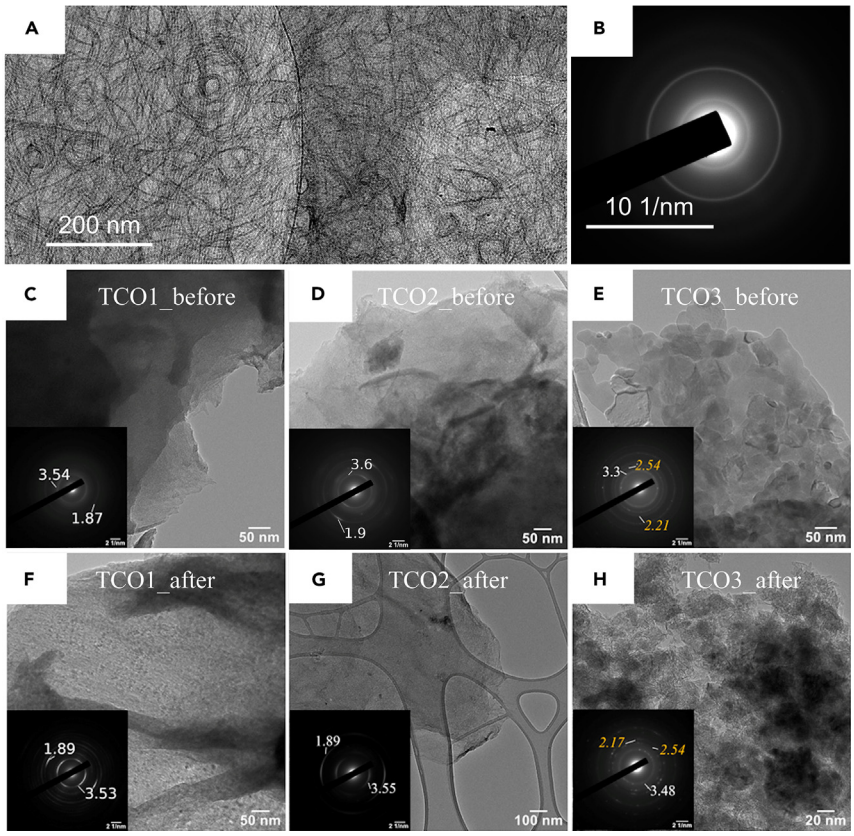

Figure 5. TEM characterization

TEM micrographs of (A) typical NFs, (B) SAD of (A), (C and D) TCO1, (E and F) TCO2, and (G and H) TCO3 samples. (A–C) before and (D–F) after, respectively, of samples exposed to Xe light in H_2O/MeOH mixtures for times listed in Table 1. Insets show SAD patterns of micrographs shown. White numbers on SAD patterns denote d-spacings in angstroms of the rings shown. Orange numbers are associated with unreacted TiC precursor. Note arcs in the majority of micrographs. The dark region in (A) is the lacey C.

common and suggest that shorter, space-filling, 1D entities are randomly oriented in the plane of the flakes. An examination of the SAD patterns reveals the presence of only two rings, with d spacings that hovered around $\approx 3.5 \pm 0.1$ and $\approx 1.9 \pm 0.1$ Å that were indexed to the (110) and (200) lepidocrocite planes, respectively.[8] The corresponding values obtained from XRD patterns (Figure 2) are 3.5 ± 0.8 and 1.89 ± 0.01 Å[7,8] and are in good agreement. The absence of any other rings confirms the 1D nature of our material. The third (002) ring is absent here, presumably because few of the NFs are oriented normal to the diffraction plane.

(2) Whenever more than two rings were observed, they could be indexed to the unreacted precursor phases, viz. TiC or Ti_3SiC_2. This is depicted in the SAD patterns in Figures 5E and 5H in orange.

(3) After the reaction, overlapping thin sheets are observed (Figures 5F–5H). The sheets are defective with a small—in the order of a few nanometers—coherence length. Small regions where the NFs are oriented in the same direction can still be observed but in a lower concentration than before photocatalysis.

(4) In general, the differences in the TEM micrographs before and after photocatalysis is not drastic, and, most importantly, the 1DL nature of our NFs is preserved.

Please cite this article in press as: Badr et al., Photo-stable, 1D-nanofilaments TiO_2-based lepidocrocite for photocatalytic hydrogen production in water-methanol mixtures, Matter (2023), https://doi.org/10.1016/j.matt.2023.05.026

(5) Last, we note that, in many regions, the 2D sheets are totally amorphous.[8]

Photocatalytic stability aspects

The most important result of this work is the extraordinary stability of our NFs under both irradiation and storage in H_2O/MeOH mixtures. As shown in Table S2, the AQYs either remain fairly constant with time or, in one case (first entry in Table S2), they increased from 4.3% to 12.6%. The simplest explanation for this increase is that our catalyst effective area increases with time as the 2D flakes disperse better and/or individual NFs (Figure 5A) become detached from others, increasing the effective area and/or the number of photocatalytically active sites.

For the most part, our first-generation materials perform significantly better than P25, a material long considered the gold standard in photocatalysis, which begs the question, why? There are at least three possible answers: (1) more light is being absorbed, and/or (2) more photochemical active sites per specific surface area exist, and/or (3) the NFs' specific surface area is quite high.

In relation to the first possible answer, since our band gap is ≈ 0.8 eV higher than that of anatase NPs, if anything, our materials should have performed worse than P25, which is not the case. Further, the presence of states in the band gap that, in turn, result in the absorption of more of the solar spectrum has been one strategy for enhancing the AQYs of photocatalysts.[17] These states can be due to defects and/or, in our case, possible C states (introduced during processing) in the band gap. When our TCOs are irradiated with a 400-nm laser (3.1 eV), sub-band-gap photoinduced excitations were observed, confirming the presence of some gap states.[18] These C states and/or defect states, in principle, should allow more of the solar spectrum to be absorbed. However, we found that H_2 production *drops* dramatically when the UV is filtered out and only visible light is used. This implies that, for unknown reasons, these localized states are *not* absorbing light and/or the electron-hole pairs generated are *not* participating in the photochemical process. At this juncture, we cannot rule out that localized states in the 3.2- to 4-eV range play a role.

Along similar lines, it is tempting to ascribe the high AQYs to the presence of Ti^{3+} cations and/or oxygen vacancies.[19,20] In this view, the EPR experiments on samples before and after photocatalysis (see Figure 4) show that, while various signals, many of which can be ascribed to Ti^{3+}, are present *before* photocatalysis, *after* photocatalysis, these signals are quenched, consistent with samples in which the only Ti oxidation state is +4. The same is true of the XPS spectra. Thus, since both EPR and XPS suggest that, if anything, the Ti^{3+} concentration decreases with time, a concomitant reduction in AQYs should have been observed. The fact that the opposite is seen (Table S2) implies this possibility can be ignored.

The second argument, having more active sites per unit surface area, is probable. At this point, we have no direct evidence for such active sites. However, if one makes the reasonable assumption that all TCOs have *comparable* surface areas, then differences in HPRs—between powders where TiB_2 was the precursor (entry 5 in Table 1) and those where TiC was the precursor (entries 2 to 4 in Table 1)—have to be ascribed to differences in active site density. This comment notwithstanding, and while it would have been useful to shed light on reaction sites and mechanisms, after decades of work, the latter remain a mystery even in well-studied materials such as P25.[21–24] Given our catalyst's 1D nature and novelty, this problem is even more acute and will require much work, which is certainly beyond the scope of this work, before clarity ensues.

Please cite this article in press as: Badr et al., Photo-stable, 1D-nanofilaments TiO_2-based lepidocrocite for photocatalytic hydrogen production in water-methanol mixtures, Matter (2023), https://doi.org/10.1016/j.matt.2023.05.026

The last argument is one of surface area. A "back-of-the-envelope" calculation of the theoretical specific surface areas of P25, with a ≈15-nm particle size[25] and NFs (5 × 7 Å^2; 1 μm long) yield values of ≈670 m^2 g^{-1} and ≈1,000 m^2 g^{-1}, respectively. In other words, all else being equal, the AQYs of our NFs should be roughly twice as high as P25. A comparison of entries 3 and 7 in Table 1 suggests the difference may be closer to an order of magnitude. If we assume the P25 Brunauer, Emmett, and Teller (BET) specific surface area of 54 m^2 g^{-1},[26] then the surface area argument is sufficient to explain our results. However, we are comparing theoretical with experimental values in the latter case. The reason theoretical values are used is that the specific surface areas obtained from BET measurements, at ≈ 10 m^2/g, are unrealistically low. This probably reflects the difficulty of the N_2 gas penetrating the NFs. This is not unique to our materials but is common, for example, in MXenes.

To show the relationship between HPRs and surface area, we placed a small piece of a filtered film of sample TCO2 in a H_2O/MeOH mixture and irradiated it. Without stirring, the HPR was 77 μmol g^{-1}·h^{-1}; with the magnetic stirrer on, it increased to 765 μmol g^{-1}·h^{-1}. In systems such as ours, where the catalyst is dispersed in a reactive liquid, an optimum catalyst concentration, which balances the penetration of the light into the suspension and the amount of catalyst, exists. Herein, this balance occurs at ≈ 1 g L^{-1} (Figure S1C). As just noted, an increase in effective surface area with time can also explain the increase in AQYs with time for the TCO2 sample (first entry in Table S2). The synthesis temperature also appears to play a role. A sample treated in TMAH at 50°C (TCO2) saw a more significant impact from the surface area. In fact, this material has been tested the most (more than 4,300 h) to demonstrate its remarkable stability under reaction conditions. Here, it is not unreasonable to assume that the 2D flakes disentangle and disperse as NFs after a specific time period.

Going back to the photocatalytic stability aspects, Table S3 and Figure S9 compare the photoactivity of our TCO materials in H_2O/MeOH mixtures with other photocatalysts exposed to light for different long-term (>20 days) irradiation times.[27–34] This comparison shows that the characteristics of our first-generation material are quite respectable, both in terms of stability and especially in terms of manufacturing costs. However, it is difficult to compare our results with others because most studies in literature are not run for prolonged irradiation times. $Rh_{2y}Cr_yO_3$/GaN:ZnO is one example of a material monitored for 180 days of irradiation time and, for longer than 90 days, it reached an AQY that was calculated to be ≈0.16% at 400–500 nm under no-stirring conditions.[34] Even so, the complex structure deactivates with time. After 180 h of irradiation time, only 50% and 20% of the initial activity were retained under no stirring and stirring during the reaction, respectively. The mechanical stirring process was also found to be an important contributor to the deactivation process, which occurs by damaging the photocatalyst surfaces. However, it does not significantly affect photoactivity when the reaction proceeds for just several days.[34,35]

Once the photoactivity stabilizes, the stirring process does not have much of an effect. In contradistinction, most TiO_2-based materials degrade after 5 days; black titania degrades after 70 h of irradiation.[20] In short, our TCO materials are among the most stable photocatalysts presented in the literature to date.

Mechanistic aspects of the photocatalytic H_2 evolution

According to the literature, oxide semiconductors have been widely used to produce H_2 through photocatalysis from aqueous MeOH solutions.[36] Even though

Please cite this article in press as: Badr et al., Photo-stable, 1D-nanofilaments TiO_2-based lepidocrocite for photocatalytic hydrogen production in water-methanol mixtures, Matter (2023), https://doi.org/10.1016/j.matt.2023.05.026

these systems are often used, there is still a great deal of mystery regarding the source of the evolved H_2 gas. Thus, the photocatalytic process is sometimes referred to as a water-splitting reaction, although others argue that it is simply a photocatalytic reforming process.[36–38] These considerations are outside the purview of this investigation. Nonetheless, we attempted to clarify the true H_2 source of select TCO samples. Consequently, isotopic labeling experiments were carried out to determine whether MeOH or water was the source of the evolved H_2 gas. When a D_2O/MeOH solution was used instead of H_2O/MeOH (see Experimental procedures section for details), the obtained thermal conductivity detector signals of H_2 and D_2 were different.[39] Moreover, the chromatographic area of D_2 was around half of the H_2 area, which implies that the source of the H_2 gas photocatalytically released from aqueous MeOH solution is indeed water.[40] However, the photo-transformation of MeOH to H_2 cannot be completely ruled out at this time. At the same time, as expected, no O_2 or CO_2 were detected either. This confirms again that the direct photocatalytic oxidation of water does not occur in MeOH. Rather, we identified methyl formate and methylal in the aqueous MeOH/H_2O solution after photocatalysis.

Following the photo-transformation process, the ultimate fate of the MeOH has to be CO_2 and H_2O. However, even after prolonged irradiation times, if CO_2 evolved, it was *below* the detectability limit of our gas chromatograph. Thus, herein MeOH is converted to chemicals other than CO_2, such as formaldehyde, methyl formate, and methylal. Similar behavior has been observed for the 2D SnS/g-C_3N_4 photocatalyst.[41] In our situation, formaldehyde synthesis was not explicitly observed (its concentration was below the detectability limit of our gas chromatography (GC). Still, its presence during the reaction helps explain why methyl formate appeared. Thus, similar to the reaction mechanism of MeOH photo-oxidation found in the literature,[41,42] at the end of the reaction, only methylal and methyl formate are found at comparable levels in the product analysis.

Because some of these chemicals are industrially useful, if they can be separated from the TCO suspensions, the green credentials and economic prospects for large-scale use of our material for green H_2 production would be significantly enhanced. In other words, if we can make useful, value-added chemicals and separate them from the water and the catalyst *without* producing CO_2, then not only is our method a CO_2-free method of making these chemicals but, as importantly, the H_2 produced would be a bonus.

Scalability and cost of raw materials

Last but not least, in regard to the scalability and cost of raw materials used in our synthesis, it should be underlined that much of previous work on H_2 production using TiO_2 has been carried out either with P25 or materials that were created by hydrothermal processing. Our approach is considerably simpler and cheaper. The process occurs at ambient pressures and temperatures <100°C, in plastic bottles shaken in a shaker oven. We recently discovered, but have not yet published the results, that we can fully convert TiB_2 powders, with ≈100% yields in 72 h, to 1D NFs under the above-mentioned conditions. This is an important discovery from a manufacturing perspective since it removes the need to separate products from reactants, which in turn greatly simplifies the manufacturing process since now centrifuges and other separation techniques are no longer required. Once the TiB_2 is converted to NFs, we simply wash the reaction mixture to remove any unreacted TMAH. Once again, we emphasize that powders of TiB_2 sell in bulk at roughly $50/kg, and all our precursors are Earth abundant and non-toxic.

Please cite this article in press as: Badr et al., Photo-stable, 1D-nanofilaments TiO_2-based lepidocrocite for photocatalytic hydrogen production in water-methanol mixtures, Matter (2023), https://doi.org/10.1016/j.matt.2023.05.026

Conclusions

In conclusion, we show that NFs obtained by reacting Ti-containing precursors, such as Ti_3SiC_2, TiC, and TiB_2, with TMAH, near ambient conditions, possess high photocatalytic activity in H_2O/MeOH mixtures (AQY, 11.7%). Impressively, the material was still active after more than 4,300 h in a 20:80 MeOH:H_2O mixture, 300 h of which were under irradiation and stirring. The material appears to be immune to stirring, and, in some cases, the AQYs increased with time. Water is the H_2 source, and neither O_2 nor CO_2 is produced. Needless to add, the absence of both gases considerably limits the number of possible reaction pathways.

The fact that our materials appear to be thermodynamically stable and photochemically active in H_2O/MeOH mixtures for extended durations cannot be overemphasized. Our findings suggest new lines for developing cheap and photo-stable materials able to produce H_2 from water for long periods of time photocatalytically. In terms of scalability, we currently routinely make 100 g/batch in a laboratory setting (see Figure S10). Since our process does not produce CO_2, its green credentials and economic prospects for significant scale-up are greatly enhanced. Furthermore, the results shown here are first generation; with better understanding of the photochemical processes, considerable progress is expected.

To sum up, these new materials meet the requirements of an efficient photocatalyst, such as effective charge separation, fast charge transfer, and, most importantly, long-term stability in aqueous environments. The present results open new avenues for the exploration of energy production systems using 1D NFs produced from cheap, non-toxic, Earth-abundant precursors using a simple, low-cost, one-pot, scalable synthesis method.

EXPERIMENTAL PROCEDURES

Resource availability

Lead contact

Further information and requests for resources and reagents should be directed to and will be fulfilled by the lead contact, Michel W. Barsoum (barsoumw@drexel.edu).

Materials availability

All structural data and information generated in this study are available from the lead contact.

Data and code availability

All data supporting the findings of this study are available within the paper and its supplemental information or from the corresponding authors upon reasonable request.

Synthesis of NFs

The details of making the NF materials can be found in an earlier article.[7] In short, TiC, Ti_3SiC_2 MAX phase, or anatase, TiO_2, powders were stirred in TMAH in polyethylene bottles in the 50°C–95°C temperature range for 3–5 days. For detailed synthesis protocols see supplemental information. After treatment in TMAH, all suspensions were collected and washed with ethanol through cycles of centrifugation and redispersion of sediments in fresh ethanol, until a pH of ≈7 was reached. After a final centrifugation step, the ethanol was decanted and MilliQ deionized (DI) water was added to the washed sediment, shaken and sonicated for 1 h in a cold bath under Ar flow, and then centrifuged at 3,500 rpm for 0.5 h to yield a stable black colloidal suspension. The latter was filtered via vacuum-assisted filtration and the

Please cite this article in press as: Badr et al., Photo-stable, 1D-nanofilaments TiO_2-based lepidocrocite for photocatalytic hydrogen production in water-methanol mixtures, Matter (2023), https://doi.org/10.1016/j.matt.2023.05.026

resulting filtered films were dehydrated in a vacuum chamber at room temperature (RT) overnight before any further characterization. When the precursor was anatase, the resulting powders were white and composed of anatase nanoparticles, not NFs.

Photocatalytic tests

For the photocatalytic tests, dry filtered films were first crushed in a mortar and pestle. In a typical experiment, 25 mg of NF powders was immersed in a cylindrical quartz reactor (with a total volume of 55 mL) containing 25 mL of a mixture of MilliQ DI water and MeOH in a 4:1 volumetric ratio, respectively. Photographs of our setup are shown in Figure S11. The reactor was equipped with two gas valves and a pressure gauge. The suspensions were magnetically stirred (700 rpm) and the reactor purged with dry nitrogen (N_2) (99.999% Linde) for at least 20 min before pressurizing to 0.2 MPa (2 bar) and irradiation for at least 5 h with UV-vis light (250–650 nm). The latter was an Asahi Spectra high-power illuminator MAX-303, with a heat-blocking design containing a 300-W xenon (Xe) light source and a UV-vis mirror module, equipped with a 1-m-long quartz light guide and a collimator lens (×1.0 Standard Type RLQL80-1), which insured that, for the most part, the irradiation was a uniform 2 suns (200 mW cm^{-2}) at a working distance of 4 cm.

AQY calculation

To calculate the AQY, using Equation 1, we used a 365-nm band-pass filter (XHQA365, Asahi Spectra) and an optical power and energy meter console (PM100D Thorlabs) equipped with a high-resolution thermal power sensor (S401C, Thorlabs). Since the Xe lamp intensity decreased with time and more than one lamp was used, the only valid comparison between runs is to compare their AQYs. The AQYs as percentages are calculated, at a wavelength of 365 nm, assuming,

$$AQY(\%) = (2 \times \#moles\ of\ H_2\ formed \times N_A \times 100) / N_{ph} \quad \text{(Equation 1)}$$

where N_A and N_{ph} are Avogadro's number and number of incident photons per second, respectively. The latter is calculated assuming:

$$N_{ph} = I^* A^* \lambda / ch \quad \text{(Equation 2)}$$

Here I, A, λ, c, and h are respectively, the light intensity, the area upon which the light is shone (1.96 cm^2), light wavelength (365 nm), at I measured, speed of light (2.988 × 10^8 m s^{-1}), and Plank's constant (6.625 × 10^{-34} J s^{-1}).

Product analysis

The gaseous samples from the outlet valve of the reactor were injected into a gas chromatograph (Shimadzu, Kyoto, Japan) coupled online with a photocatalytic reactor, equipped with a thermal conductivity detector (TCD) for the quantification of H_2 and other gases and a flame ionization detector (FID) for identification of other organic compounds. Two parallel-coupled GC columns, a MolSieve 5A (column length of 30 m and internal diameter [ID] of 0.32 mm) and a Rt-Q-Bond (column length of 30 m and ID of 0.53 mm) were used. The gas chromatograph was calibrated by injecting H_2 and Ar mixtures (purchased from Linde) of known proportions. The reproducibility of the data was checked by performing independent experiments in duplicate, by which consistent results were obtained with dispersions <5%. Crucially, no CO_2 was detected during the reaction.

Blank tests

Different blank control measurements were performed both in the absence of the photocatalyst and with the hole scavenger (MeOH), and no H_2 or O_2 were detected even after 6 h of irradiation. Other control tests were also conducted, under dark

Please cite this article in press as: Badr et al., Photo-stable, 1D-nanofilaments TiO_2-based lepidocrocite for photocatalytic hydrogen production in water-methanol mixtures, Matter (2023), https://doi.org/10.1016/j.matt.2023.05.026

conditions, by immersing photocatalysts in the H_2O/MeOH mixture. Again, no H_2 was produced in the absence of light. This demonstrates that H_2 production does not proceed without the presence of a photocatalyst. As importantly, when the UV part of the spectrum was filtered out, little H_2 was produced.

Time dependence of H_2 production

The temporal evolution of H_2 production over long irradiation times was carried out using the same setup, quantities of reaction mixture (25 mL of DI water and MeOH with a volumetric ratio of 4:1), and solid material (25 mg) following the same procedure described above for the detection of evolved H_2 gas. After a designated reaction time, the entire gas content of the reactor was injected into the GC in order to quantify the H_2. The reactor was then re-pressurized to 2 bar with dry N_2 and the process repeated. To measure the long-term stability in the H_2O/MeOH mixtures, in some cases, after the a few initial runs, where the H_2 was quantified, the reaction vessel was detached from the light source and stored, unstirred, in a dark hood, at RT, for times ranging from 1 to 6 months. Sporadically, the reaction vessel was taken out from the dark, illuminated by the Xe lamp for a predetermined time, and the H_2 produced quantified. In some cases, this process was repeated a few times. During these tests, the contents of the vessel were stirred.

Cyclic tests

To perform this type of experiment, after each 18 h of reaction (taking a gas sample every 6 h), the photocatalyst was recovered by vacuum filtration and then reintroduced inside the reactor for the next cycle. Each cycle used the same reaction conditions specified above.

Experiments with heavy water

In order to explore whether the source of H_2 was from water splitting and not from MeOH, in one set of parallel experiments under the same reaction conditions and light intensities outlined above, we replaced the DI water with D_2O (99.9%, Deutero), again with MeOH as scavenger.

Materials characterization

XRD

Powder XRD patterns were collected using a diffractometer (Bruker-AXS D8 Advance equipped with a LynxEye 1D detector), a Cu Kα (0.1541 nm) radiation source, and a scintillation counter detector. The diffraction patterns were recorded in a 2θ angle range of 5°–90°, with a step size of 0.02° and a rate of 1.2° min^{-1}. For the most part, the XRD patterns were obtained on powders. Before illumination, the NFs were crushed in a mortar and pestle for a few minutes. After exposure to the Xe lamp, storing in the dark, etc., the solids were recovered from the suspensions by vacuum-assisted filtration, dried (vacuum chamber at RT overnight), and re-crushed in a mortar and pestle for a few minutes. The XRD patterns were obtained from these powders. This was done to break up any agglomerates that formed during the test. Needless to add, the agglomerates must have reduced our AQYs. In the future, a deflocculant may be added to the mixture to prevent agglomeration.

UV-vis spectroscopy

The UV-vis spectroscopy was carried out in diffuse reflectance (DR) mode. Measurements were carried out on a spectrophotometer (Lambda 45 PerkinElmer) equipped with an RSA-PE-20 integration sphere. All DR UV-vis spectra were recorded under ambient conditions in the 200- and 700-nm range using $BaSO_4$ as baseline. The spectra were collected in reflectance units and converted into the Kubelka-Munk

Please cite this article in press as: Badr et al., Photo-stable, 1D-nanofilaments TiO_2-based lepidocrocite for photocatalytic hydrogen production in water-methanol mixtures, Matter (2023), https://doi.org/10.1016/j.matt.2023.05.026

remission function F(R). Before each measurement, equal amounts by weight of finely granulated 1DL samples and $BaSO_4$ powders were mixed and loaded in a quartz cell with Suprasil windows. The band gap energy was determined by finding the intercept of the straight line in the low-energy rise of a plot of $[F(R) \cdot h\nu]^2$ against $h\nu$, where ν is the incident photon energy and h is Plank's constant.

Raman spectroscopy

Raman spectra were recorded in the 50- and 2,000-cm^{-1} range using a spectrometer (HORIBA Jobin-Yvon LabRAM HR Evolution) equipped with an air-cooled CCD (charge coupled device) and a 633-nm He-Ne laser. The spectra were recorded in the extended scan mode at RT. To avoid sample degradation, the laser power (9.7 mW) was adjusted by using different neutral-density filters. We note in passing that it is important to acquire Raman spectra with low laser power; high power transforms the lepidocrocite to anatase.[8]

EPR

The EPR measurements were carried out using a spectrometer (Continuous Wave X-Band Bruker EMX plus) equipped with a resonator (Bruker X-SHQ 4119HS-W1 X-Band). The measurement parameters for the X-Band measurements were as follows: microwave frequency, 9.877 GHz; microwave power, 0.63 mW; modulation amplitude, 0.2 mT; conversion time, 20.02 ms; time constant, 10.24 ms with three scans.

TEM

The morphological changes occurring in our TCOs as a result of immersion in the H_2O/MeOH solution and exposure to the Xe light were followed using a transmission electron microscope, TEM, (JEOL 2100, equipped with high-resolution polar piece). The samples were crushed when needed, dispersed in ethanol, and drop cast on a 400-mesh lacey carbon (C) grid.

XPS

For the XPS measurements, we used a spectrometer (Kratos XPS Axis Ultra DLD Setup) using Al Kα (1486.74 eV) radiation produced by an X-ray source operating at a total power of 300 W (12.0 kV × 25 mA) and a vacuum of $\sim 1 \times 10^{-4}$ MPa. The emitted photoelectrons were recorded using a 165-mm radius hemispherical energy analyzer operated in a fixed analyzer transmission mode with a pass energy of 20 eV and a magnetic immersion lens for enhancing the electron detection efficiency. Additionally, an electron flood gun operating at 1-eV electron energy and a 0.1-mA current was used to compensate for sample charging effects. The above parameters were optimized in order to obtain the adventitious C 1s peak at 285 ± 0.05 eV.

SUPPLEMENTAL INFORMATION

Supplemental information can be found online at https://doi.org/10.1016/j.matt.2023.05.026.

ACKNOWLEDGMENTS

This work was funded by the Division of Materials Research of the National Science Foundation (grant # 2211319). Financial support from the Romanian Ministry of Research, Innovation, and Digitization through the Core Program 2023–2026 (contract PC3-PN23080303) is gratefully acknowledged. This work was partially supported by grants of the Ministry of Research, Innovation and Digitization, CNCS-UEFISCDI,

project numbers PN-III-P4-PCE-2021-1461 and PN-III-P4-ID-ERC-2021-0007, all within PNCDI III. This work is also supported by the CSIR-NCL startup fund.

AUTHOR CONTRIBUTIONS

H.O.B., methodology, writing – review & editing; V.N., methodology, investigation, writing – review & editing; S.N., conceptualization, methodology, writing – review & editing, supervision, project administration; F.N., methodology, investigation, writing – review & editing; A.C.N., methodology, investigation, writing – review & editing; A.M.R., methodology, investigation, writing – review & editing; M.R., methodology, investigation; M.W.B., conceptualization, methodology, writing – review & editing, supervision, project administration; M.F., conceptualization, methodology, writing – review & editing, supervision, project administration.

DECLARATION OF INTERESTS

A provisional patent application on the preparation and use of TCOs for H_2 production from water entitled "Catalytic production of hydrogen from water" naming S.N., M.F., and M.W.B. was recently filed.

Received: February 3, 2023
Revised: April 17, 2023
Accepted: May 16, 2023
Published: June 9, 2023

REFERENCES

1. Suess, H.E., and Urey, H.C. (1956). Abundances of the elements. Rev. Mod. Phys. *28*, 53–74. https://doi.org/10.1103/RevModPhys.28.53.

2. Neaţu, Ş., Puche, M., Fornés, V., and Garcia, H. (2014). Cobalt-containing layered or zeolitic silicates as photocatalysts for hydrogen generation. Chem. Commun. *50*, 14643–14646. https://doi.org/10.1039/C4CC05931J.

3. Jiao, Y., Zheng, Y., Jaroniec, M., and Qiao, S.Z. (2015). Design of electrocatalysts for oxygen- and hydrogen-involving energy conversion reactions. Chem. Soc. Rev. *44*, 2060–2086. https://doi.org/10.1039/C4CS00470A.

4. Tee, S.Y., Win, K.Y., Teo, W.S., Koh, L.-D., Liu, S., Teng, C.P., and Han, M.-Y. (2017). Recent progress in energy-driven water splitting. Adv. Sci. *4*, 1600337. https://doi.org/10.1002/advs.201600337.

5. Tong, H., Ouyang, S., Bi, Y., Umezawa, N., Oshikiri, M., and Ye, J. (2012). Nano-photocatalytic materials: possibilities and challenges. Adv. Mater. *24*, 229–251. https://doi.org/10.1002/adma.201102752.

6. Wen, J., Xie, J., Chen, X., and Li, X. (2017). A review on g-C_3N_4-based photocatalysts. Appl. Surf. Sci. *391*, 72–123. https://doi.org/10.1016/j.apsusc.2016.07.030.

7. Badr, H.O., El-Melegy, T., Carey, M., Natu, V., Hassig, M.Q., Johnson, C., Qian, Q., Li, C.Y., Kushnir, K., Colin-Ulloa, E., et al. (2022). Bottom-up, scalable synthesis of anatase nanofilament-based two-dimensional titanium carbo-oxide flakes. Mater. Today *54*, 8–17. https://doi.org/10.1016/j.mattod.2021.10.033.

8. Badr, H.O., Lagunas, F., Autrey, D.E., Cope, J., Kono, T., Torita, T., Klie, R.F., Hu, Y.-J., and Barsoum, M.W. (2023). On the structure of one-dimensional TiO_2 lepidocrocite. Matter *6*, 128–141. https://doi.org/10.1016/j.matt.2022.10.015.

9. Sasaki, T., Watanabe, M., Michiue, Y., Komatsu, Y., Izumi, F., and Takenouchi, S. (1995). Preparation and acid—base properties of a protonated titanate with the lepidocrocite-like layer. Chem. Mater. *7*, 1001–1007.

10. Tauc, J., Grigorovici, R., and Vancu, A. (1966). Optical properties and electronic structure of amorphous germanium. phys. stat. sol. *15*, 627–637. https://doi.org/10.1002/pssb.19660150224.

11. Makuła, P., Pacia, M., and Macyk, W. (2018). How to correctly determine the band gap energy of modified semiconductor photocatalysts based on UV–vis spectra. J. Phys. Chem. *9*, 6814–6817. https://doi.org/10.1021/acs.jpclett.8b02892.

12. Urbach, F. (1953). The long-wavelength edge of photographic sensitivity and of the electronic absorption of solids. Phys. Rev. *92*, 1324. https://doi.org/10.1103/PhysRev.92.1324.

13. Hu, W., Li, L., Li, G., Liu, Y., and Withers, R.L. (2014). Atomic-scale control of TiO_6 octahedra through solution chemistry towards giant dielectric response. Sci. Rep. *4*, 6582–6589.

14. Orton, J.W., Auzins, P., and Wertz, J.E. (1960). Double-quantum electron spin resonance transitions of nickel in magnesium oxide. Phys. Rev. Lett. *4*, 128–129. https://doi.org/10.1103/PhysRevLett.4.128.

15. Scheibe, B., Tadyszak, K., Jarek, M., Michalak, N., Kempiński, M., Lewandowski, M., Peplińska, B., and Chybczyńska, K. (2019). Study on the magnetic properties of differently functionalized multilayered $Ti_3C_2T_x$ MXenes and Ti-Al-C carbides. Appl. Surf. Sci. *479*, 216–224. https://doi.org/10.1016/j.apsusc.2019.02.055.

16. Bodziony, T., Kaczmarek, S.M., Tran, V.H., Figiel, P., Biedunkiewicz, A., and Leniec, G. (2018). Magnetic properties of AISI 316L stainless steel doped with nanocrystalline Ti–B–C powders. Mater. Res. Express *5*, 126105. https://doi.org/10.1088/2053-1591/aae115.

17. Doustkhah, E., Assadi, M.H.N., Komaguchi, K., Tsunoji, N., Esmat, M., Fukata, N., Tomita, O., Abe, R., Ohtani, B., and Ide, Y. (2021). In situ Blue titania via band shape engineering for exceptional solar H_2 production in rutile TiO_2. Appl. Catal. B Environ. *297*, 120380. https://doi.org/10.1016/j.apcatb.2021.120380.

18. Colin-Ulloa, E., Martin, J.L., Hanna, R.J., Frasch, M.H., Ramthun, R.R., Badr, H.O., Uzarski, J.R., Barsoum, M.W., Grimm, R.L., and Titova, L.V. (2023). Electronic structure of 1D lepidocrocite TiO_2 quat-derived nanomaterial, QDN, as revealed by optical absorption and photoelectron spectroscopy. J. Phys. Chem. C *127*, 7275–7283. https://doi.org/10.1021/acs.jpcc.2c06719.

19. Mohajernia, S., Andryskova, P., Zoppellaro, G., Hejazi, S., Kment, S., Zboril, R., Schmidt, J., and Schmuki, P. (2020). Influence of Ti^{3+} defect-type on heterogeneous photocatalytic H_2 evolution activity of TiO_2. J. Mater. Chem. *8*, 1432–1442. https://doi.org/10.1039/C9TA10855F.

20. Chen, X., Liu, L., Yu, P.Y., and Mao, S.S. (2011). Increasing solar absorption for photocatalysis with black hydrogenated titanium dioxide

nanocrystals. Science *331*, 746–750. https://doi.org/10.1126/science.1200448.

21. Schneider, J., Matsuoka, M., Takeuchi, M., Zhang, J., Horiuchi, Y., Anpo, M., and Bahnemann, D.W. (2014). Understanding TiO_2 photocatalysis: mechanisms and materials. Chem. Rev. *114*, 9919–9986. https://doi.org/10.1021/cr5001892.

22. Linsebigler, A.L., Lu, G., and Yates, J.T. (1995). Photocatalysis on TiO_2 surfaces: principles, mechanisms, and selected results. Chem. Rev. *95*, 735–758. https://doi.org/10.1021/cr00035a013.

23. Wang, Q., and Domen, K. (2020). Particulate photocatalysts for light-driven water splitting: mechanisms, challenges, and design strategies. Chem. Rev. *120*, 919–985. https://doi.org/10.1021/acs.chemrev.9b00201.

24. Maeda, K., and Domen, K. (2010). Photocatalytic water splitting: recent progress and future challenges. J. Phys. Chem. Lett. *1*, 2655–2661. https://doi.org/10.1021/jz1007966.

25. Tobaldi, D.M., Pullar, R.C., Seabra, M.P., and Labrincha, J.A. (2014). Fully quantitative X-ray characterisation of evonik aeroxide TiO_2 P25. Mater. Lett. *122*, 345–347.

26. Wang, X., Pehkonen, S.O., Rämö, J., Väänänen, M., Highfield, J.G., Laasonen, K., Yang, Q.f., and Ren, Y. (2012). Experimental and computational studies of nitrogen doped Degussa P25 TiO_2: application to visible-light driven photo-oxidation of as (iii). Catal. Sci. Technol. *2*, 784–787.

27. Xie, M.Y., Su, K.Y., Peng, X.Y., Wu, R.J., Chavali, M., and Chang, W.C. (2017). Hydrogen production by photocatalytic water-splitting on Pt-doped TiO_2–ZnO under visible light. J. Taiwan Inst. Chem. Eng. *70*, 161–167. https://doi.org/10.1016/j.jtice.2016.10.034.

28. Goto, Y., Hisatomi, T., Wang, Q., Higashi, T., Ishikiriyama, K., Maeda, T., Sakata, Y., Okunaka, S., Tokudome, H., Katayama, M., et al. (2018). A particulate photocatalyst water-splitting panel for large-scale solar hydrogen generation. Joule *2*, 509–520. https://doi.org/10.1016/j.joule.2017.12.009.

29. Lyu, H., Hisatomi, T., Goto, Y., Yoshida, M., Higashi, T., Katayama, M., Takata, T., Minegishi, T., Nishiyama, H., Yamada, T., et al. (2019). An Al-doped $SrTiO_3$ photocatalyst maintaining sunlight-driven overall water splitting activity for over 1000 h of constant illumination. Chem. Sci. *10*, 3196–3201. https://doi.org/10.1039/C8SC05757E.

30. Hara, M., Kondo, T., Komoda, M., Ikeda, S., Kondo, J.N., Domen, K., Hara, M., Shinohara, K., and Tanaka, A. (1998). Cu_2O as a photocatalyst for overall water splitting under visible light irradiation. Chem. Commun. 357–358. https://doi.org/10.1039/A707440I.

31. Maeda, K., Teramura, K., Lu, D., Takata, T., Saito, N., Inoue, Y., and Domen, K. (2006). Photocatalyst releasing hydrogen from water. Nature *440*, 295. https://doi.org/10.1038/440295a.

32. Zhang, G., Lan, Z.-A., Lin, L., Lin, S., and Wang, X. (2016). Overall water splitting by Pt/g-C_3N_4 photocatalysts without using sacrificial agents. Chem. Sci. *7*, 3062–3066. https://doi.org/10.1039/C5SC04572J.

33. Liu, J., Liu, Y., Liu, N., Han, Y., Zhang, X., Huang, H., Lifshitz, Y., Lee, S.T., Zhong, J., and Kang, Z. (2015). Metal-free efficient photocatalyst for stable visible water splitting via a two-electron pathway. Science *347*, 970–974. https://doi.org/10.1126/science.aaa3145.

34. Ohno, T., Bai, L., Hisatomi, T., Maeda, K., and Domen, K. (2012). Photocatalytic water splitting using modified GaN:ZnO solid solution under visible light: long-time operation and regeneration of activity. J. Am. Chem. Soc. *134*, 8254–8259. https://doi.org/10.1021/ja302479f.

35. Maeda, K., Teramura, K., Masuda, H., Takata, T., Saito, N., Inoue, Y., and Domen, K. (2006). Efficient overall water splitting under visible-light irradiation on $(Ga_{1-x}Zn_x)(N_{1-x}O_x)$ dispersed with Rh−Cr mixed-oxide nanoparticles: effect of reaction conditions on photocatalytic activity. J. Phys. Chem. B *110*, 13107–13112. https://doi.org/10.1021/jp0616563.

36. Kheradmand, A., Zhu, Y., Gu, S., and Jiang, Y. (2021). Photocatalytic hydrogen evolution. In Solar-to-Chemical Conversion: Photocatalytic and Photoelectrochemcial Processes, pp. 77–105. https://doi.org/10.1002/9783527825073.ch4.

37. Cargnello, M., Gasparotto, A., Gombac, V., Montini, T., Barreca, D., and Fornasiero, P. (2011). Photocatalytic H_2 and added-value by-products – the role of metal oxide systems in their synthesis from oxygenates. Eur. J. Inorg. Chem. *2011*, 4309–4323. https://doi.org/10.1002/ejic.201100532.

38. Ma, J., Liu, K., Yang, X., Jin, D., Li, Y., Jiao, G., Zhou, J., and Sun, R. (2021). Recent advances and challenges in photoreforming of biomass-derived feedstocks into hydrogen, biofuels, or chemicals by using functional carbon nitride photocatalysts. ChemSusChem *14*, 4903–4922. https://doi.org/10.1002/cssc.202101173.

39. Silvestri, M., and Adorni, N. (1956). Continuous measurement of deuterium concentration in hydrogen by means of thermal conductivity. Rev. Sci. Instrum. *27*, 388–391. https://doi.org/10.1063/1.1715581.

40. Kandiel, T.A., Ivanova, I., and Bahnemann, D.W. (2014). Long-term investigation of the photocatalytic hydrogen production on platinized TiO_2: an isotopic study. Energy Environ. Sci. *7*, 1420–1425. https://doi.org/10.1039/C3EE41511B.

41. Uddin, N., Langley, J., Zhang, C., Fung, A.K., Lu, H., Yin, X., Liu, J., Wan, Z., Nguyen, H.T., Li, Y., et al. (2021). Zero-emission multivalorization of light alcohols with self-separable pure H_2 fuel. Appl. Catal. B Environ. *292*, 120212. https://doi.org/10.1016/j.apcatb.2021.120212.

42. Bhattacharyya, K., Tripathi, A.K., Gupta, N.M., and Tyagi, A.K. (2010). Photodegradation of methanol under UV–visible irradiation by titania dispersed on polyester cloth. Photochem. Photobiol. *86*, 241–246. https://doi.org/10.1111/j.1751-1097.2009.00653.x.